Deposition in the tungsten divertor during the 2011–2016 campaigns in JET with ITER-like wall

N Catarino[1] ⓘ**, A Widdowson**[2] ⓘ**, A Baron-Wiechec**[2] ⓘ**, J P Coad**[2]**,**
K Heinola[3,4] ⓘ**, M Rubel**[5] ⓘ**, N P Barradas**[1,6] ⓘ**, E Alves**[1] ⓘ **and JET**
Contributors[7]

[1] IPFN, Instituto Superior Técnico, Universidade de Lisboa, 1049-001, Lisboa, Portugal
[2] Culham Centre for Fusion Energy, Culham Science Centre, Abingdon, OX14 3DB, United Kingdom
[3] University of Helsinki, PO Box 64, FI-00560 Helsinki, Finland
[4] Nuclear Data section, Division of Physical and Chemical Sciences, International Atomic Energy Agency,
PO Box 100, A-1400, Austria
[5] Royal Institute of Technology, Association EURATOM-VR, SE-100 44 Stockholm, Sweden
[6] C2TN, Instituto Superior Técnico, Universidade de Lisboa, E.N. 10, Sacavém 2686-953, Portugal

E-mail: norberto.catarino@ctn.tecnico.ulisboa.pt

CrossMark

Abstract

A build-up of co-deposits in remote areas of the divertor can contribute significantly to the overall fuel retention. The control of plasma-material interactions via the study and understanding of erosion-deposition of PFCs provides vital information for the efficient future operation of ITER. The major aim of this work is to reveal details of beryllium deposition and fuel (deuterium) retention on divertor plasma-facing componentsremoved from the JET ITER-Like Wall divertor after cumulative exposure during the first two (ILW$-1 + 2$) and all three (ILW$-1 + 2 + 3$) campaigns. Ion beam analysis techniques such as Rutherford backscattering spectrometry, nuclear reaction analysis and proton induced x-ray emission have been extensively used for post-mortem analyses of selected tiles from JET following each campaign and can provide relevant information on plasma-surface interactions like tungsten erosion, beryllium deposition and plasma fuel retention with divertor tiles via implantation or co-deposition. The studied divertor tiles represent a unique set of samples, which have been exposed to plasmas since the beginning of the JET-ILW operation for three successive plasma campaigns. This is a comprehensive comparison of divertor components after these operation periods. The results presented summarise deposition and fuel retention on Tiles 4 (inner base) and 6 (outer base). Although the deposition pattern is similar to that determined after individual campaigns, D retention is not a cumulative process and is determined mainly by the last campaign, and the total Be deposit after the 3 campaigns (i.e. data $1 + 2 + 3 =$ tile exposed 2011–2016) is less than the sum of the deposits after each individual campaign (sum $1 + 2 + 3$) for Tile 4 but greater for Tile 6.

Keywords: JET, plasma-material interaction, tokamaks, ion beam analysis, deposition, tungsten, beryllium

(Some figures may appear in colour only in the online journal)

1. Introduction

Material erosion, migration and fuel inventory in JET are carried out using beryllium (Be) and tungsten (W) marker tiles and several types of wall probes installed in the main
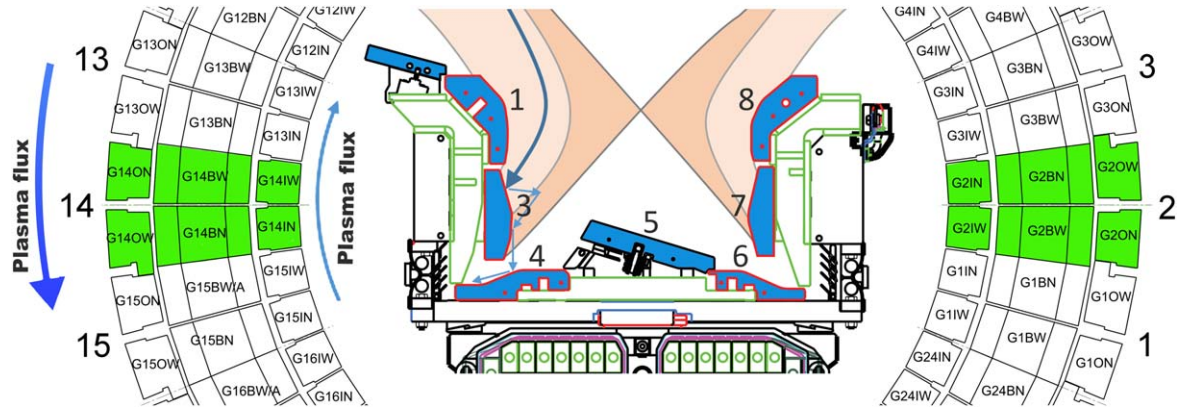
Figure 1. Schematics illustration of JET-ILW divertor tile arrangement toroidally, and a cross-section of the JET-ILW divertor with the tle number and a typical plasma equilibrium. The blue arrows indicate the direction of the plasma flux.

chamber and in the divertor [1]. Post-mortem analyses of these diagnostic samples after three campaigns with the ITER-Like Wall (JET ILW) reveal the main transport and retention mechanism in the PFC surfaces [2–17]. During the limiter plasma phase, the plasma will be in contact with the plasma facing limiters, leading to the erosion of Be limiters in the main chamber, and local redeposition. During the divertor phase particles eroded in the main chamber can enter the plasma or the scrape off layer (SOL) and migrate around the edge of the plasma to the divertor giving rise to deposition, primarily at the top of tiles 0 and 1 [5, 16].

For JET the impurities consisted primarily of Be and after being transported to divertor areas and stick at the landing spot. For ILW-2 and 3 campaigns the inner strike-point distribution extended beyond Tile 3 onto Tile 4, so that the deposition area expanded onto Tile 3. After Be reaches the divertor region, it can migrate into the plasma shadowed zone in a step-by-step process, eroding from one point and re-depositing onto a nearby area. At the same time, deuterium (D), the plasma fuel, can be co-deposited with the Be and other impurities such as carbon (C) and oxygen (O) detected in the shadowed zones, and can thus reach remote areas of the divertor. Therefore the re-deposition of these impurities can lead to the formation of hydrogen-rich layers [18], which is an issue of concern from the viewpoint of tritium (T) inventory as well as hydrogen recycling during the discharge.

This study presents the results from ion beam analysis (IBA) for fuel retention and deposition patterns on Tiles 4 (inner base) and 6 (outer base) of the JET divertor during the first three ILW campaigns, and compares with the cumulative deposit after the three campaigns (i.e. data 1 + 2 + 3 = tile exposed 2011–2016).

2. Experimental details

A selection of passive diagnostic components and marker tiles was installed in JET during each shutdown between operating campaigns. The JET-ILW divertor is divided into 8 octants, each composed of 2 modules, resulting in a total of 16 modules, the numerical identification of each of the modules
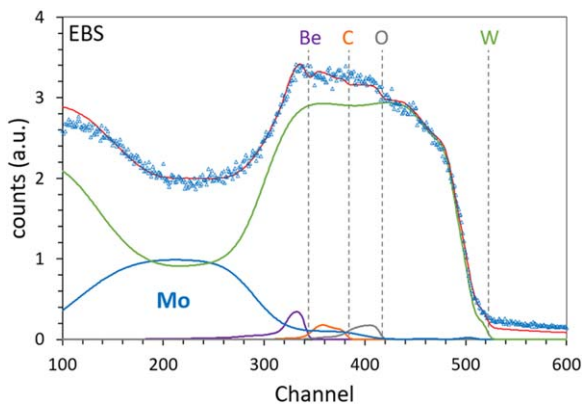
is represented in figure 1, the diverter is further separated into 3 main zones: in the inner divertor are Tiles 0, 1 and 3; in the base are tiles 4, 5 and 6, and in the outer divertor are tiles 6, 7 and 8. Each of the modules is subdivided 2 sides, being in the ccw direction designated: narrow and wide. Since a module can have 4 tiles of a certain type, each tiles are also designated by A, B, C and D, in ccw order. So when we refer to the tile '14BN G4D', we are referring to tile 4 in module 14, in the base of the diverter, narrow side and position D. The material transport to remote and inaccessible areas happen in a multi-step process, this designation also allows us to easily identified the tiles, which will most contribute to impurities is the analyse tile. In this case of the Tile 14BN G4D, the poloidal component of the plasma flux will carry impurities from tile '14IN G3B' [19]. Table 1, identify all the tiles used in this work, as well the period in vessel and the main tile for the source of impurity's and their period in the vessel. The S-coordinate system have been discussed by several authors [5, 7, 14]. and represents a poloidal trajectory following the tile surfaces, starting at the upper left corner of the High Field Gap Closure tile (Tile 0) and following the tile surfaces from the inner to the outer divertor [5–7].

It should be noted that tiles do not come always from the same module, but from opposite modules, and may be some asymmetry in the toroidal deposition. A complete description of the sample handling from JET-ILW and preparation of laboratory samples for surface analysis and characterisation has been presented by Widdowson *et al* [20].

The tiles are solid structures with ∼25 μm W coatings with a 3 μm Molybdenum (Mo) interlayer layer over carbon fibre composite substrates (W-CFC) shaped to maximise their power handling capabilities. This introduces some difficulties in mounting each tile for IBA, which were overcome by measuring each of the flat segments separately. In this work we will focus on the results of divertor Tiles 4 and 6, coated with a W marker layer with a thickness of about 3 μm and a 3 μm thick molybdenum (Mo) interlayer between the W marker layer and the thick W coating [21]. The Mo interlayer is necessary to distinguish the W marker layer from the W coating for depth profiling methods, therefore enabling the erosion of W to be measured and the quantitative determination of deposition of all
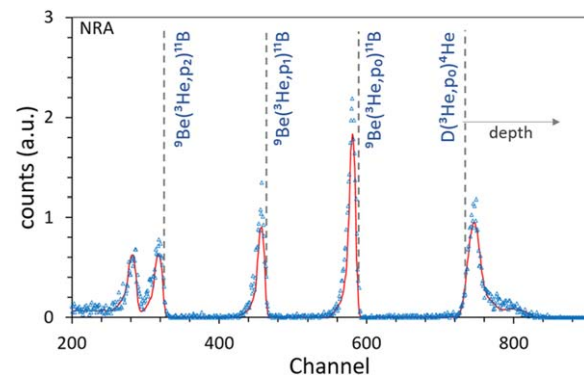
Table 1. List of sample used for this study, in vessel period, and neighbouring tile.

| Tile name | Coating | In vessel period | | | Faces | |
		ILW I	ILW II	ILW III	Tile name	in Vessel
14BN G4D	Marker	✓			14IN G3B	ILW I
14BN G4D	Marker		✓		14IN G3B	ILW I + II
2BN G4C	Standard			✓	2IN G3B	ILW I + II + III
2BN G4D	Standard	✓	✓	✓	2IN G3B	ILW I + II + III
2BN G6C	Marker	✓			2OW G7B	ILW I
2BN G6C	Marker		✓		2OW G7B	ILW I + II
14BN G6D	Standard			✓	14OW G7B	ILW I + II + III
14BN G6D	Marker	✓	✓		14OW G7B	ILW I + II
2BN G6C	Standard		✓	✓	2OW G7B	ILW I + II + III
2BN G6D	Standard	✓	✓	✓	2OW G7B	ILW I + II + III

Figure 2. Representative EBS spectra of Tile 6 after the JET-ILW-3 comapain, at the bottom of the sloping region ($S = 1470$).

Figure 3. Typical NRA spectra spectra of Tile 6 after the JET-ILW-3 comapain, at the bottom of the sloping region ($S = 1470$).

elements. The data presented for Tile 4 and 6 that were in the vessel for more than one campaign were standard W-coated tiles used only for studying deposition since the erosion studies with IBA techniques are not possible in this case.

Be and D deposition was analysed by IBA techniques using the 2.5 MV Van de Graaff accelerator installed at Laboratory of Accelerators and Radiation Technologies of Instituto Superior Técnico. Analyses of JET tiles were performed in a chamber dedicated to fusion research, where samples, including full JET tiles, contaminated with tritium and beryllium can be handled. A particle detector for Rutherford backscattering (RBS) is located at a scattering angle of $150°$. The detector for nuclear reaction analysis (NRA) is placed at a $135°$ scattering angle. It has an active layer with 2 mm thickness to detect the protons from $D(^3He,p)^4He$ reaction that have 12.5 MeV energy. A particle filter in front of the NRA detector, with a 140 μm thick Al, absorb the scattered primary ions and the 14 MeV α particles from $^9Be(^3He, \alpha_0)^8Be$. The characteristic x-rays were detected with a Si(Li) detector placed at a $150°$ scattering angle, with a particle filter with a 350 μm thick Mylar, to absorb the scattered primary ions. Elastic backscattering spectrometry (EBS) and particle induced x-ray emission (PIXE) were performed with 2.3 MeV incident protons. RBS and NRA were performed using ^3He ions at an energy of 2.3 MeV in order to measure the amounts of ^2H (D), Be and C.

The $D(^3He,p)^4He$ reaction was used to measure the D content, the $^9Be(^3He,p_x)^{11}B$ ($x = 0, 1, 2, 3$) reactions for Be and the $^{12}C(^3He,p_0)^{14}N$ reaction for ^{12}C. For thin deposits, the NRA data provide more sensitive and accurate results for Be and C than the RBS data, which are used for thick deposits. At 2.3 MeV the NRA cross-section for carbon is very low, and in the case of thick films the signal from C ($^{12}C(^3He,p_0)^{14}N$) overlaps with the Be signal ($^9Be(^3He,p_3)^{11}B$), limiting its detection. Non-Rutherford elastic scattering and nuclear cross sections of 0.5–2.35 MeV p and ^3He in beryllium have been measured for this geometry [22, 23] in order to make possible to discriminate the signals resulting from backscattering of heavy elements and Be elastic and inelastic nuclear reactions, as can be seen in figure 2, where small amount of Be can be fit and provide a better element profile. Cross sections for $D(^3He,p)^4He$ reaction are calculated internally by NDF code, following the expression of by Möller and Besenbacher [24].

The tiles were analysed using EBS, RBS, NRA and PIXE, in the poloidal direction every 5 mm along the tile surface using a 1 mm beam spot size to have a complete picture of the composition. The experimental data were analysed using the NDF code [25] to quantify all the impurities present in the tiles. Representative EBS and NRA spectra for the bottom of the sloping region ($S = 1470$) of Tile 6 after the JET-ILW-3 campaign are shown in figures 2 and 3, the red curve represents the best fit obtained with the NDF code. The
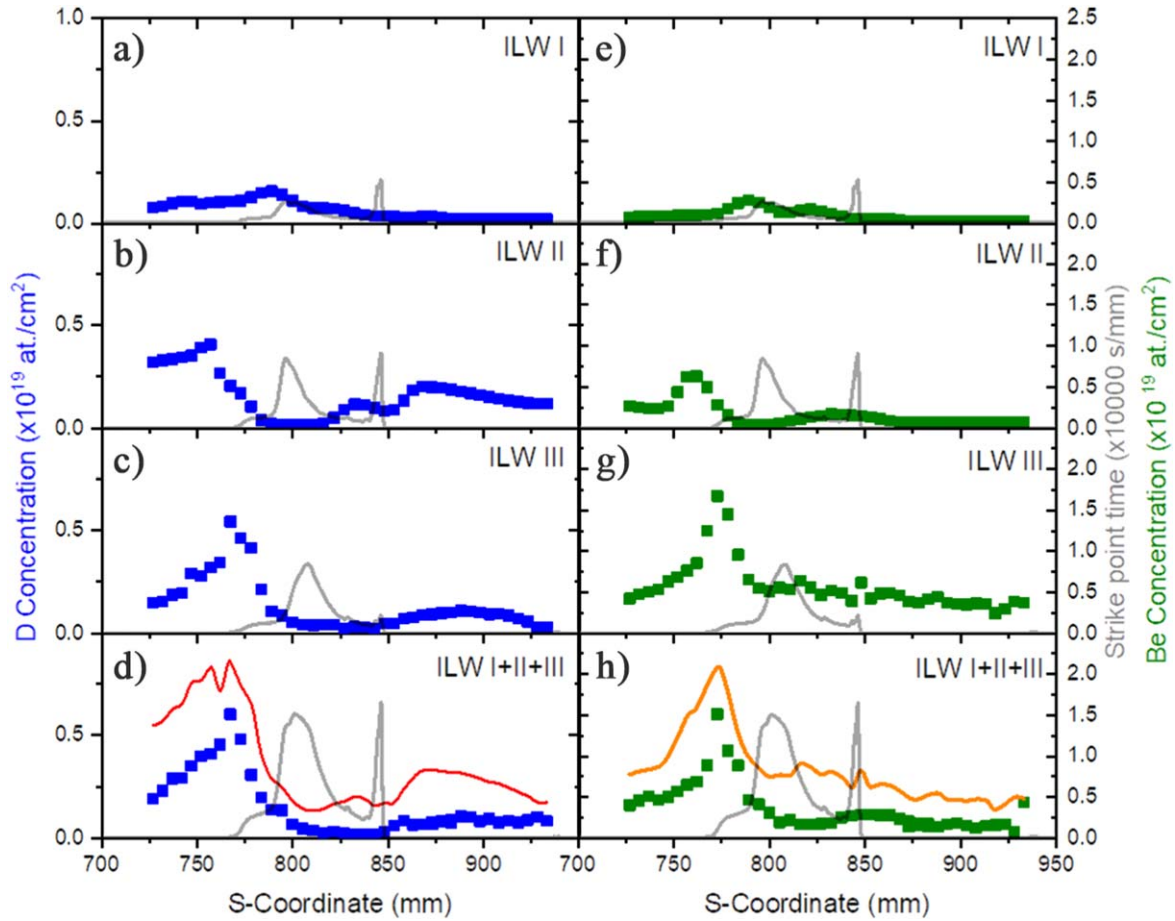
Figure 4. Deposition of D (blue) and Be (green) on Tile 4. Red and orange line represents the sum of the deposits of D and Be in individual campaigns. Grey line is strike point distribution for the ILW-1 to ILW-3 and for the three campaigns.

sample composition is determined in a self-consistent way with PIXE data simulated by means of the LibCPIXE code [26]. The PIXE data were analysed with the GUPIX code [27] and the results used as input for NDF-LibCPIXE.

3. Results

The analyses of the divertor tile, and despite the differences of strikes point position and input energies, share similar deposition pattern for all ILW campaigns; more than 50% of the total deposition is always observed in tiles 0 and 1, additional deposit zones were observed in the button part of the slope of tiles 4 and 6. Deposits contain mainly of Be with some D and C [7, 16, 28], in the same areas, oxygen was also observed, possibly due to oxidation of Be layers after contact with atmospheric air.

The C concentration reduce by a factor of about 2 from campaign JET-ILW1 to JET-ILW2 from JET-ILW2 to JET-ILW3 the reduction of the C concentration is less significant. The high C concentration measure in JET-ILW1 can be explained by C that remaining from JET-C, the source of the remaining C in ILW-2 and ILW-3 could potentially be eroded from back and sides of divertor tiles, made of CFC material not protected by W coating.

The total D accumulation in the divertor remained roughly constant for all three campaigns, The decrease of D concentration from JET-ILW1 to JET-ILW2 is mainly because of the last discharges in ILW-2campaign, that ended with discharges in H. We can also attribute this decrease of D to the decrease in C concentration, however, the D concentration increasing from JET-ILW2 to JET-ILW3 indicates that co-deposition with C impurities is not the significant source of D accumulation in JET-ILW divertor for JET-ILW2 and JET-ILW3, and D accumulation is mainly co-deposition with Be. And in this work we will focus only in the distribution of these two elements.

On Tile 4 deposits rich in D, Be are observed in the plasma shadowed surface, i.e. the flat region of the tile below the slope ($s = 713$–762 mm). During X-point plasmas neutrals erode Be from the inner wall [29]. Eroded Be becomes ionised and is transported through the SOL [30] and is deposited in the divertor together with D and other impurities. The evidence of this transport mechanism is the direct correlation between the strike point time distribution and the amount of Be deposit on Tile 4; in JET-ILW-2 and 3 the time of the strike point located on Tile 4 increases and the Be deposition also increased in this region, as can be seen in figures 4(e)–(c). After the initial transport to the plasma accessible surface of the tile, the deposited material is sputtered and redeposited in a step-by-step process until it
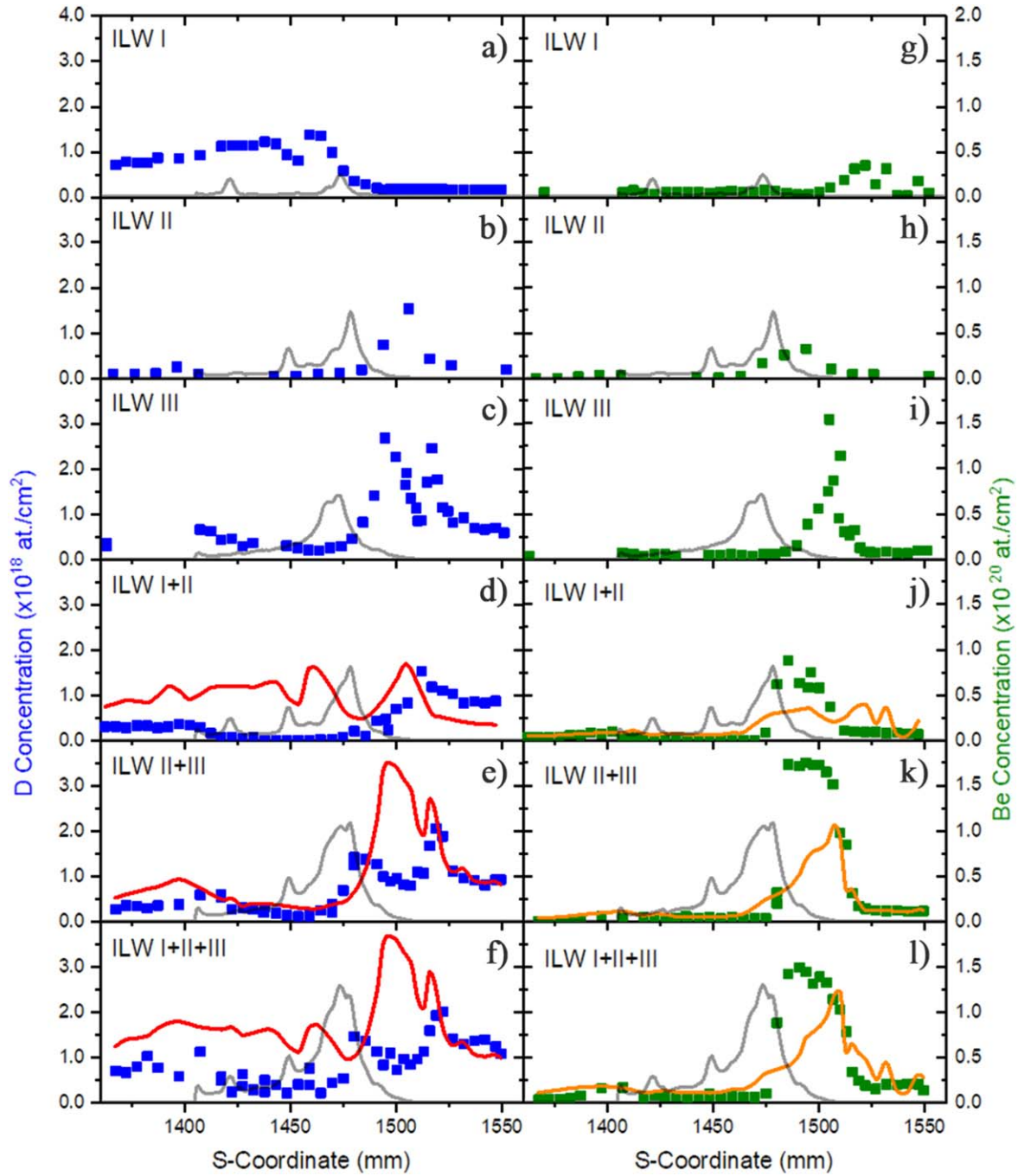
Figure 5. Deposition of D (blue) and Be (green) on Tile 6. Red and orange line represents the sum of the deposits of D and Be in individual campaigns. Grey line is strike point distribution for the ILW-1 to ILW-3 and for the three campaigns.

migrates to the remote inner corner. This can be seen in [7] where the Be thickness in the plasma accessible region ($s > 775$ mm) is nearly one order of magnitude lower than in the remote area ($s < 775$ mm). This is also the reason why the Tile exposed over three campaigns shows a similar amount of Be deposit (figure 4(h)) to that after campaign ILW-3 (figure 4(g)) in the plasma accessible region and an increase in the remote area. However, the deposit never reaches the sum of the three individual campaigns, because the pre-existing Be from the previous campaign is transported to even more remote zones of the divertor. The reason for the reduction of the Be deposit on the

tile that was in the vessel for three campaigns at the top of the sloping part ($s > 850$ mm) is not clear, particularly as this is in the private flux region, but the retention of D is also reduced. A more detailed study is necessary to explain this behaviour, using a modelling of impurity transport code like the ERO2.0 code [31].

The increase of the strike point times on Tile 4 during the ILW-2 and 3 campaigns lower the D content in the plasma accessible surface due to heating of the surface [30], as shown in figures 4(a)–(c). This heating of the surface leads to increased desorption of the D, and since the third campaign is

the longest and containing the most powerful plasma pulses leads to the D retention in the tile exposed for three campaign being very close to the amount in the tile exposed only during ILW-3, as shown in figures 4(a)–(d).

Deposition of D, Be , C and O are also detected in the plasma shadowed outer corner of Tile 6. The Be content is ∼5 times greater than on Tile 4 and ∼5 times higher than on Tile 6 after the ILW-2 campaign [11]. The differences in the Be amount and profile [16] between campaigns is due to an increase in the time of the outer strike point on Tile 6, that is ∼4 times longer in ILW-2 and 3 than in ILW-1 as shown in figures 5(a)–(c). On Tile 6 the deposition was inhomogeneous with deposition predominantly at the bottom of the sloping region in a band from $s \approx 1480$ mm to $s \approx 1515$ mm. In the plasma-shadowed area of Tile 6 the D, C and O are present [7] but at lower concentrations than observed in the plasma-shadowed area of Tile 4, nevertheless the deposition mechanism in this zone should be the same. The combination of increased strike point time and the lower threshold energy of C and O compared with Be increases the number of cycles of erosion/deposition for these elements and extends their range leading to less deposition on the outboard end of Tile 6, but more deposition deeper into the corner region. In contrast to what happens in the inner divertor the outer strike point was often positioned on tile 6, and the lower area of Tile 7 also experienced significant fluxes from the SOL [5] resulting in some Be accumulation. It is noticeable that the Tile 6 in vessel for more than one campaign show a richer Be deposit than the sum of tiles exposed to the individual campaigns. It may be that deposition on Tile 7 also contributes to deposition on Tile 6 in subsequent campaigns via erosion/deposition steps. When a marker Tile 6 is exchanged for a fresh tile for the next campaign, the Tile 7 is also exchanged for a new tile, with the exception of the end of the second campaign, where tile 7 has not been replaced, this is probably the reason for the increase in the deposit of Be in ILW-3. However, a Tile 6 exposed to more than one campaign would be adjacent to a Tile 7 that had not been replaced at between shutdowns. Thus it may be that the Tile 6 exposed for multiple campaigns benefits from an additional source of Be on the adjacent Tile 7, which may explain why a Tile 6 exposed to more than one campaign has more Be deposit than the sum of the Be on the tiles from individual campaigns.

It should be noted that the total Be in the deposit region can be underestimated, since with a beam energy of 2.3 MeV we can only determine the composition of the first 2×10^{20} at cm^{-2} of sample (∼16.6 μm for pure Be). On the Tiles 6 exposed to a single campaign, in the plasma shadowed area, the amount of D co-deposited with the Be was greatest following ILW-3, as shown in figure 5(c). This follows the pattern for other tiles, and is unsurprising since ILW-2 ended with discharges in H and ILW-1 was less extensive. However, for tiles exposed for more than one campaign the D concentration is similar to that of the last campaign (figures 5(d)–(f)); this may be due to the thickness of deposit since the analysis depth for D is less than 10 μm.

On the upper horizontal surface of the Tile 6 ($s = 1363$–1425 mm) the amount of D decreases an order to $\sim 10^{17}$ at cm^{-2}. This surface was partly shadowed by Tile 5 and was in the private flux region when the strike point was on Tile 6.

4. Conclusion

The deposition of Be and D in the JET divertor during each of the first three ITER-like wall campaigns (ILW-1, ILW-2 and ILW-3) show similar deposition patterns. In the remote inner corner of the divertor (Tile 4) fuel retention is an order of magnitude higher (∼5.0×10^{18} at cm^{-2} of D) than the maximum deposition seen near the bottom of the sloping surface (∼0.5×10^{18} at cm^{-2} of D), i.e. $s > 770$ mm. The D retention on a Tile 4 exposed for the three campaigns (i.e. data $1 + 2 + 3 =$ tile exposed 2011–2016) follows the pattern of the last campaign i.e. ILW-3. The same happens for fuel retention at the outer corner (Tile 6), i.e. the deposition pattern is similar to that of the last campaign, suggesting that there is no cumulative effect.

The maximum Be deposited in Tile 4 increases ∼x5 going from ILW-1 to ILW-2 and ILW-33, reaching a total of 1.5×10^{19} at cm^{-2}, beyond the predominant strike point position (770 mm $< s <$ 798 mm), mainly because of changes in the strike point distribution between the campaigns. The same thing happens on Tile 6: the outer strike point was located on Tile 6–4 times longer in ILW-2 and 3 than during ILW-1. The Be deposition is predominantly at the bottom of the sloping region in a band from $s \approx 1480$ mm to $s \approx 1515$ mm. For tiles in vessel for more than one campaign the Be deposit is greater than the sum of single campaign deposits. We assume that this is because of the contribution to Be deposition in the course of the various campaigns arising from Tile 7. D and Be concentration for tiles in vessel for more than one campaign can be underestimated, IBA analysis with high ion energy will be beneficial for a better estimation of deposits in Tile 6.

For the comparing deposition pattern we use the time the strike point, however this do not give any information plasma flux, or ion energy that vary from l-mode to H-mode and during ELMs. It would be helpful estimate incident ion flux in the diverter region, for example using, Langmuir probes or spectroscopy as proposal by the or of Guillemaut *et al* [32].

ORCID iDs

N Catarino ⓘ https://orcid.org/0000-0003-3879-1533
A Widdowson ⓘ https://orcid.org/0000-0002-6805-8853
A Baron-Wiechec ⓘ https://orcid.org/0000-0001-9458-6679
K Heinola ⓘ https://orcid.org/0000-0002-0601-8274
M Rubel ⓘ https://orcid.org/0000-0001-9901-6296
N P Barradas ⓘ https://orcid.org/0000-0001-7795-8573
E Alves ⓘ https://orcid.org/0000-0003-0633-8937

References

[1] Rubel M *et al* 2013 Overview of erosion–deposition diagnostic tools for the ITER-like wall in the JET tokamak *J. Nucl. Mater.* **438** S1204–7

[2] Koivuranta S, Likonen J, Hakola A, Coad J P, Widdowson A, Hole D E and Rubel M 2014 Post-mortem measurements of fuel retention at JET *Phys. Scr.* **T159** 014052

[3] Widdowson A *et al* 2014 Material migration patterns and overview of first surface analysis of the JET ITER-like wall *Phys. Scr.* **T159** 014010

[4] Catarino N, Widdowson A, Baron-Wiechec A, Coad J P, Heinola K, Rubel M and Alves E 2017 Time-resolved deposition in the remote region of the JET-ILW divertor: measurements and modelling *Phys. Scr.* **2017** T170

[5] Widdowson A *et al* 2017 Overview of the JET ITER-like wall divertor *Nucl. Mater. Energy* **12** 499–505

[6] Heinola K *et al* 2017 Experience on divertor fuel retention after two ITER-Like Wall campaigns *Phys. Scr.* **T170** 014063

[7] Catarino N, Barradas N P, Corregidor V, Widdowson A, Baron-Wiechec A, Coad J P, Heinola K, Rubel M and Alves E 2017 Assessment of erosion, deposition and fuel retention in the JET-ILW divertor from ion beam analysis data *Nucl. Mater. Energy* **12** 559–63

[8] Heinola K, Likonen J, Ahlgren T, Brezinsek S, De Temmerman G, Jepu I, Matthews G F, Pitts R A, Widdowson A and Contributors J 2017 Long-term fuel retention and release in JET ITER-Like Wall at ITER-relevant baking temperatures *Nucl. Fusion* **57** 086024

[9] Widdowson A *et al* 2019 Deposition of impurity metals during campaigns with the JET ITER-like Wall *Nucl. Mater. Energy* **19** 218–24

[10] Baron-Wiechec A *et al* 2015 Global erosion and deposition patterns in JET with the ITER-like wall *J. Nucl. Mater.* **463** 157–61

[11] Petersson P, Rubel M, Esser H G, Likonen J, Koivuranta S and Widdowson A 2015 Co-deposited layers in the divertor region of JET-ILW *J. Nucl. Mater.* **463** 814–7

[12] Heinola K *et al* 2015 Fuel retention in JET ITER-Like Wall from post-mortem analysis *J. Nucl. Mater.* **463** 961–5

[13] Krat S, Gasparyan Y, Pisarev A, Bykov I, Mayer M, de Saint Aubin G, Balden M, Lungu C P and Widdowson A 2015 Erosion at the inner wall of JET during the discharge campaign 2011–2012 in comparison with previous campaigns *J. Nucl. Mater.* **456** 106–10

[14] Heinola K *et al* 2016 Long-term fuel retention in JET ITER-like wall *Phys. Scr.* **T167** 014075

[15] Likonen J, Heinola K, De Backer A, Koivuranta S, Hakola A, Ayres C F, Baron-Wiechec A, Coad J P, Matthews G F, Mayer M and Widdowson A 2016 Deuterium trapping and release in JET ITER-like wall divertor tiles *Phys. Scr.* **T167** 014074

[16] Mayer M *et al* 2016 Erosion and deposition in the JET divertor during the first ILW campaign *Phys. Scr.* **T167** 014051

[17] Widdowson A *et al* 2017 Impurity re-distribution in the corner regions of the JET divertor *Phys. Scr.* **T170** 014060

[18] Likonen J *et al* 2019 Investigation of deuterium trapping and release in the JET ITER-like wall divertor using TDS and TMAP *Nucl. Mater. Energy* **19** 166–78

[19] Brezinsek S 2015 Plasma-surface interaction in the Be/W environment: conclusions drawn from the JET-ILW for ITER *J. Nucl. Mater.* **463** 11–21

[20] Widdowson A *et al* 2016 Experience of handling beryllium, tritium and activated components from JET ITER like wall *Phys. Scr.* **T167** 014057

[21] Ruset C, Grigore E, Munteanu I, Maier H, Greuner H, Hopf C, Phylipps V and Matthews G 2009 Industrial scale 10 μmW coating of CFC tiles for ITER-like Wall Project at JET *Fusion Eng. Des.* **84** 1662–5

[22] Catarino N, Barradas N P and Alves E 2016 Determination of ^{9}Be(p,p$_0$) ^{9}Be, ^{9}Be(p,d$_0$) ^{8}Be and ^{9}Be(p,α_0) ^{6}Li cross sections at 150° in the energy range 0.5–2.35 MeV *Nucl. Instrum. Methods Phys. Res.* B **371** 50–3

[23] Barradas N P, Catarino N, Mateus R, Magalhães S, Alves E, Siketić Z and Radović I B 2015 Determination of the ^{9}Be(^{3}He,$_{pi}$)^{11}B ($i = 0, 1, 2, 3$) cross section at 135° in the energy range 1–2.5 MeV *Nucl. Instrum. Methods Phys. Res.* B **346** 21–5

[24] Möller W and Besenbacher F 1980 A note on the 3He + D nuclear-reaction cross section *Nucl. Instrum. Methods* **168** 111–4

[25] Barradas N P and Jeynes C 2008 Advanced physics and algorithms in the IBA DataFurnace *Nucl. Instrum. Methods Phys. Res.* B **266** 1875–9

[26] Pascual-Izarra C, Barradas N P and Reis M A 2006 LibCPIXE: A PIXE simulation open-source library for multilayered samples *Nucl. Instrum. Methods Phys. Res.* B **249** 820–2

[27] Maxwell J A, Teesdale W J and Campbell J L 1995 The Guelph PIXE software package II *Nucl. Instrum. Methods Phys. Res.* B **95** 407–21

[28] Mayer M, Krat S, Baron-Wiechec A, Gasparyan Y, Heinola K, Koivuranta S, Likonen J, Ruset C, de Saint-Aubin G and Widdowson A 2017 Erosion and deposition in the JET divertor during the second ITER-like wall campaign *Phys. Scr.* **T170** 014058

[29] Brezinsek S *et al* 2015 Beryllium migration in JET ITER-like wall plasmas *Nucl. Fusion* **55** 063021

[30] Sugiyama K, Porosnicu C, Jacob W, Jepu I and Lungu C P 2016 Investigation of deuterium retention in/desorption from beryllium-containing mixed layers *Nucl. Mater. Energy* **6** 1–9

[31] Romazanov J *et al* 2017 First ERO2.0 modeling of Be erosion and non-local transport in JET ITER-like wall *Phys. Scr.* **T170** 014018

[32] Guillemaut C *et al* 2016 Experimental estimation of tungsten impurity sputtering due to Type I ELMs in JET-ITER-like wall using pedestal electron cyclotron emission and target Langmuir probe measurements *Phys. Scr.* **T167** 014005